JCTC Journal of Chemical Theory and Computation

Discrete Variable Representation Implementation of the One-Electron Polarization Model

Tae Hoon Choi,[†] Thomas Sommerfeld,[‡] S. Levent Yilmaz,[†] and Kenneth D. Jordan*,[†]

Department of Chemistry, University of Pittsburgh, Pittsburgh, Pennsylvania 15260, Southeastern Louisiana University, Hammond, Louisiana 70402, and Center for Simulation and Modeling, University of Pittsburgh, Pittsburgh, Pennsylvania 15260

Received May 18, 2010

Abstract: A discrete variable representation (DVR) implementation of an one-electron polarization model (OPEM) for characterizing $(H_2O)_n^-$ clusters is described. For the $(H_2O)_{90}^-$ cluster, evaluation of the energy and gradient using a suitable DVR basis sets is about a 2 orders of magnitude faster than corresponding calculations using a Gaussian orbital basis set. The DVR version of the code has been parallelized using OpenMP to enable molecular dynamics (MD) simulations of large $(H_2O)_n^-$ clusters.

1. Introduction

The interaction of excess electrons with water clusters has been the subject of numerous experimental and theoretical studies.[1–40] A key to much of the computational work in this area has been the development of the electron−water potentials for use in one-electron model Hamiltonians.[27–40] Our group has introduced both a quantum Drude oscillator approach[33,34] and a computationally simpler one-electron polarizable model (OEPM)[39] for describing $(H_2O)_n^-$ clusters. The GTO implementation of the OEPM model, including the evaluation of analytical gradients, has been described in earlier publications.[39,41]

When using Gaussian type orbital (GTO) basis sets, the construction of the matrix elements $\mathbf{H}_{kl} = \int \varphi_k^*(x)\mathbf{H}\varphi_l(x)\mathrm{d}x$ is the major time-consuming part of the calculation of the energy and of the analytical gradients. We consider here an alternative approach involving the discrete variable representation (DVR) method.[42–56] Although the use of the DVR basis sets results in much larger Hamiltonian matrices, the matrix elements are rapid to evaluate, and the sparsity of the matrices allows for rapid diagonalization. In the following section, we describe the DVR implementation of the OEPM algorithm and compare its performance with the GTO implementation for $(H_2O)_n^-$ clusters with n as large as 90. We note that Jacobson and Herbert have also used a DVR approach for calculating the electron binding energies of their one-electron polarization model.[40] However, there are several differences between the two approaches, making a detailed examination of a DVR approach to our one-electron model instructive. Parallelization of the OEPM-DVR code using shared memory and OpenMP[57] is also described.

2. Computational Methods

2.1. DVR with the OEPM Hamiltonian. The OEPM method is built on top of the DPP water model developed in our group.[58] In this model, each water monomer carries three point charges, $+Q$ at each H atom and $-2Q$ at a so-called M site located 0.25 Å from the O atom on the rotational axis and displaced toward the H atoms. In the DPP model, each atom is polarizable, with Thole-type[59] damping of the charge-induced dipole and induced dipole−induced dipole interactions. Finally, there are exponential repulsive interactions between atoms of different monomers and attractive van der Waals interactions between the O atoms. In the OEPM method, the model Hamiltonian (in atomic units) for an excess electron interacting with a water cluster is

$$\mathbf{H} = -\frac{1}{2}\nabla^2 - \sum_i \frac{Q_i}{r_i} f_{\mathrm{pc}}(r_i) + \sum_j V_j^{\mathrm{rep}} + \sum_j \frac{\boldsymbol{\mu}_j \cdot \mathbf{r}_j}{r_j^3} f_{\mathrm{ind}}(r_j) - \sum_j \frac{\alpha}{2r_j^4} f_{\mathrm{pol}}(r_j) \quad (1)$$

* To whom correspondence should be addressed: E-mail: jordan@pitt.edu.

[†] University of Pittsburgh.

[‡] Southeastern Louisiana University.

10.1021/ct100263r
Published on Web 07/12/2010

where the first sum is over the charge sites in the DPP model, and the third term represents a short-ranged repulsive potential (V_{rep}), expanded in terms of six *s* GTOs on each monomer. The sums in the fourth and fifth terms, which correspond to the interaction of the excess electron with the induced dipoles (from the water−water interactions) and the induced dipoles from the electron−water interaction, are over the *M* sites. (Although each water molecule employs three polarizable sites for the water−water interaction, only a single polarizable site is used for the electron−water interaction. This reduces the computational effort while having little impact on the accuracy of the model.) It should be noted that for computational efficiency we have collapsed the induced dipoles on the atoms of each monomer to the associated *M* site. The f_{pc}, f_{ind}, and f_{pol} damping functions are represented as $f_{pc}(r_i) = 1 - \exp(-b_1 r_i^2)$, $f_{ind}(r_j) = (1 - \exp(-b_2 r_j^2))^2$, and $f_{pol}(r_j) = (1 - \exp(-b_3 r_j^2))^2$, respectively. The f_{pc} damping term is employed in the DVR but not in the GTO version of the code.

The DVR method is well documented in the literature,[42–50] and only a brief summary is given here. We adopt the sine DVR approach, which uses particle-in-a-box eigenfunctions as a basis. For simplicity we describe the DVR method for one-dimensional case; extension to three dimensions is straightforward. The underlying basis functions for the sine DVR method are

$$\varphi_j(x) = \begin{cases} \sqrt{\frac{2}{L}}\sin\left(\frac{j\pi(x - x_0)}{L}\right) & \text{for } x_0 \le x \le x_{n+1} \\ 0 & \text{otherwise} \end{cases} \quad (2)$$

where x_0 and x_{n+1} refer to the box edges and $L = x_{n+1} - x_0$. The DVR kinetic energy matrix elements can be evaluated analytically by transforming to eigenfunctions of the position operator expressed in terms of the φ_j. In this new basis

$$\mathbf{T}_{kl}^{DVR} = -\left(\frac{\pi(n+1)}{L}\right) \times \begin{cases} \frac{1}{3} + \frac{1}{6(n+1)^2} - \frac{1}{2(n+1)^2\sin^2\left(\frac{k\pi}{n+1}\right)} & \text{if } k = l \\ \frac{2(-1)^{k-1}}{(n+1)^2} \frac{\sin\left(\frac{k\pi}{n+1}\right)\sin\left(\frac{l\pi}{n+1}\right)}{\left(\cos\left(\frac{k\pi}{n+1}\right) - \cos\left(\frac{l\pi}{n+1}\right)\right)^2} & \text{if } k \ne l \end{cases} \quad (3)$$

With a δ function basis set, the potential energy matrix would be diagonal. In the finite basis sets used in actual applications, the eigenfunctions of the position operator approximate delta functions. Thus, for sufficiently large DVR basis sets, to a good approximation one can treat *V* as diagonal. For sine DVR basis sets, the diagonal elements of *V* are defined at the *n* uniformly spaced grid points $\{x_i\}$, where *n* is the number of sine functions in the basis set. The total Hamiltonian matrix for the 3-dimensional case has the form

$$\tilde{\mathbf{H}} = \begin{pmatrix} 3N^{4/3} \\ \text{nonzero elements} \end{pmatrix} + \begin{pmatrix} V(q_1) & 0 & 0 & 0 & \cdots & 0 \\ 0 & V(q_2) & 0 & 0 & \cdots & 0 \\ 0 & 0 & V(q_3) & 0 & \cdots & 0 \\ 0 & 0 & 0 & V(q_4) & \cdots & 0 \\ \vdots & \vdots & \vdots & \vdots & \ddots & \vdots \\ 0 & 0 & 0 & 0 & \cdots & V(q_N) \end{pmatrix} \quad (4)$$

where *N* is the total number of DVR grid points ($N = n \times n \times n$), and q_i denotes a point on the three-dimensional grid. The kinetic energy matrix has $3N^{4/3}$ nonzero elements. The resulting $N \times N$ Hamiltonian matrix is very sparse, and the eigenvalue equation, $\mathbf{HC} = \varepsilon C$, is solved using iterative Lanczos diagonalization.[60]

2.2. Analytical Gradients in the DVR Method. In the DVR approach the gradient of the energy assumes a particularly simple form since there are no Pulay terms,[61,62] and the kinetic energy terms do not contribute. The gradient is thus given by

$$\frac{\partial E}{\partial R} = (C_1 \; C_2 \; C_3 \; \cdots \; C_N) \times \begin{pmatrix} \frac{\partial V(q_1)}{\partial R} & 0 & 0 & \cdots & 0 \\ 0 & \frac{\partial V(q_2)}{\partial R} & 0 & \cdots & 0 \\ 0 & 0 & \frac{\partial V(q_3)}{\partial R} & \cdots & 0 \\ \vdots & \vdots & \vdots & \ddots & \vdots \\ 0 & 0 & 0 & \cdots & \frac{\partial V(q_N)}{\partial R} \end{pmatrix} \begin{pmatrix} C_1 \\ C_2 \\ C_3 \\ \vdots \\ C_N \end{pmatrix} = \sum_{i=1}^{N} \frac{\partial V(q_i)}{\partial R} C_i^2 \quad (5)$$

where the C_i are the coefficients of the converged wave function.

2.3. Box Size and Grid Points. In the applications of the OEPM-DVR method to $(H_2O)_n^-$ clusters, it is important to choose appropriate box sizes and grid point spacing. This can be especially challenging for excess electron systems as the spatial extent of the excess electron can vary appreciable, depending on the arrangement of the water monomers. To illustrate the issues at play we consider the two $(H_2O)_6^-$ clusters and the two $(H_2O)_{45}^-$ clusters shown in Figure 1. One $(H_2O)_6^-$ structure (A) binds the excess electron by about 0.6 eV and the other (B) binds it by only ~0.1 eV. Both $(H_2O)_{45}^-$ structures strongly bind the excess electron, but one has it bound on the surface and the other in the interior. The geometries of the clusters were taken from ref 39.

3. Results

3.1. Convergence with Box Size and Density of Grid Points. The first set of exploratory calculations employed a cubic box of 30 bohr size and 1 bohr spacing of the grid points. In these and all other calculations carried out in this study, the

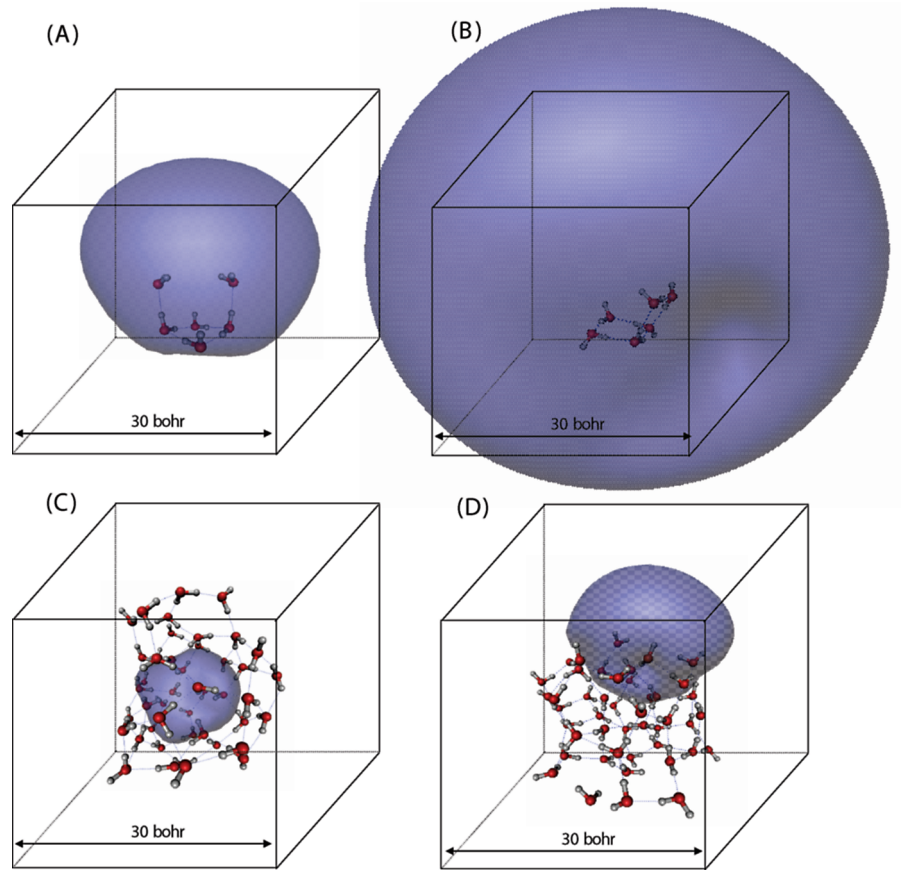

Figure 1. Isosurface containing 90% of the excess electron density calculated by the OEPM-GTO method are plotted for two $(H_2O)_6^-$ and two $(H_2O)_{45}^-$ clusters.

center of the cubic grid of DVR points was located at the center of mass of the cluster. For each of the four test systems the surface enclosing 90% of the density of the excess electron was calculated. The results are shown in Figure 1 from which it is immediately clear that the 30 bohr box is too small for the weak electron binding $(H_2O)_6^-$ species (B) but that it should be appropriate for the two $(H_2O)_{45}^-$ for which the excess electron is much more localized. One cannot tell from this figure alone as to whether this box size is suitable for the $(H_2O)_6^-$ (A) species.

In Figure 2 the electron binding energies of the four test systems are plotted as a function of the number of grid point (n) along one dimension of the cubic box for box lengths of 30, 60, and 90 bohr. For the 30 bohr box, the binding energies are relatively constant as n varies from 30 to 110, but for the larger boxes, the binding energies show appreciable oscillations for grids with spacings between the points greater than about 1.5 bohr. Clearly for convergence of the energies one needs to employ grids with spacings less than this. We also checked the convergence of the forces and find that in most cases, there are well converged for DVR basis sets that correspond to a grid spacings of ≤ 1 bohr.

From Figure 2, it is also seen that the excess electron is not even bound for $(H_2O)_6^-$ (B) when the 30 bohr box is used and that the use of this small box size leads to a sizable error in the EBE of the more strongly bound $(H_2O)_6^-$ species as well. The 30 bohr box, however, is suitable for the two $(H_2O)_{45}^-$ isomers, and the 60 bohr box is suitable for obtaining well converged EBE's for all four of the test systems.

4. Performance of the DVR Method

In evaluating the performance of the DVR method for describing $(H_2O)_n^-$ ions, comparison is made with the timings for calculations using a Gaussian-type basis set which has been optimized for use with the OEPM method.[39] This basis set employs three s and one p function on each water monomer and a 5s 4p set of GTOs at the center of mass of the cluster. Figure 3 reports the CPU time for the evaluation of the energy and gradient of clusters containing two to 90 water molecules with the DVR and the GTO basis sets. DVR results are reported for $30 \times 30 \times 30$, $60 \times 60 \times 60$, and $90 \times 90 \times 90$ grids. The energy and gradient evaluations with the GTO basis set both display $O(M^{2.9})$ scaling, where M is the number of monomers, whereas the corresponding DVR calculations essentially display $O(M^{1.0})$ and $O(M^{1.4})$ scaling, respectively. The weaker scaling in the DVR case is a consequence of the fact that the number of DVR grid points was not increased with increasing the number of molecules. Of course for very large clusters, if one did not know in advance where the electron is localized, it would be necessary to adopt larger DVR grids. For the $60 \times 60 \times 60$ grid, the energy plus gradient calculations with the DVR basis set are faster than calculations with the GTO basis set for $M \geq 17$.

With the DVR basis set, the most time-consuming part of the energy calculation is the diagonalization of the Hamiltonian matrix. Thus, the CPU time for the energy calculation in the DVR basis set depends mainly on the number of grid points, and only weakly (linearly) on the number of water

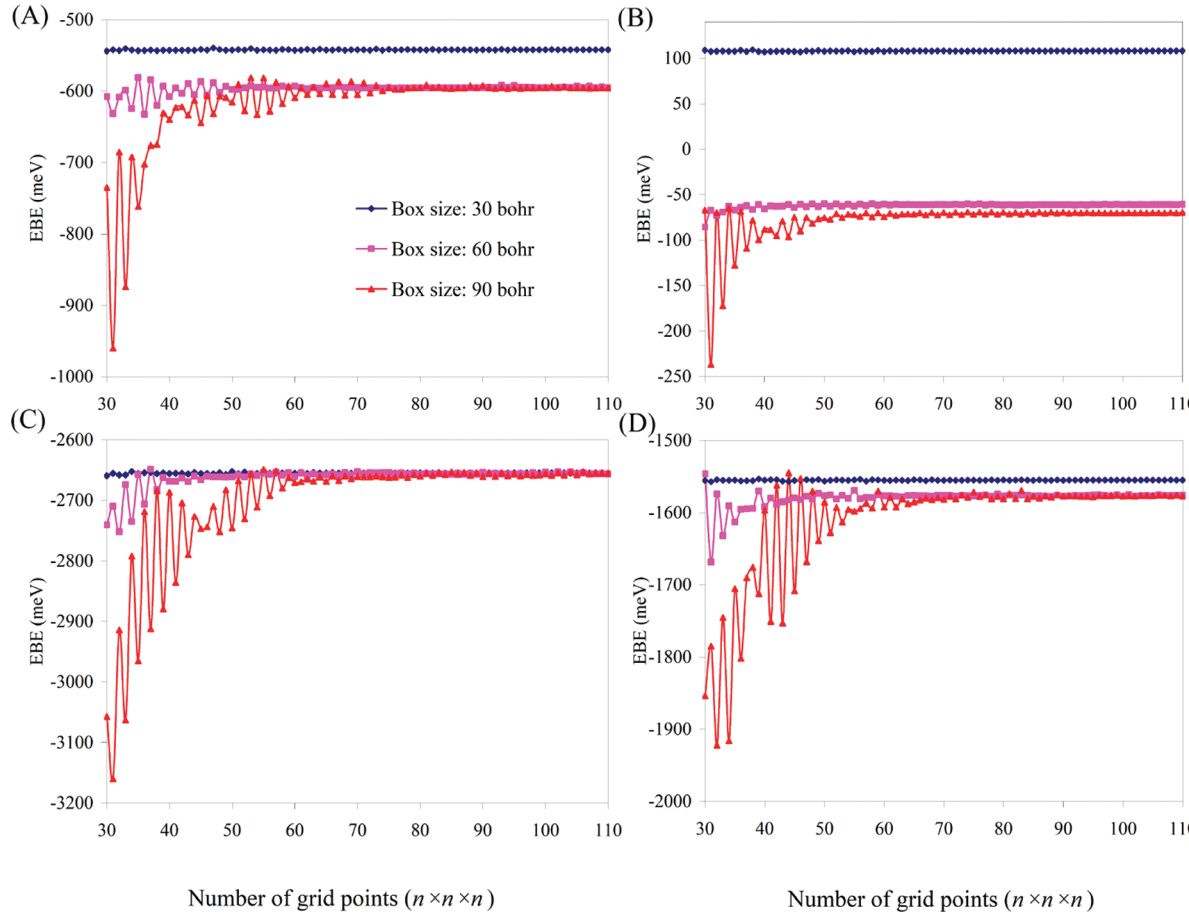

Figure 2. Electron binding energies of the four $(H_2O)_n^-$ clusters shown in Figure 1. Results are reported for 30 × 30 × 30, 60 × 60 × 60, and 90 × 90 × 90 bohr box sizes. The number of grid points in each dimension is varied from 30 to 110.

molecules (see Figures 3 and 4). For the gradient evaluations with the DVR method, there is a slightly stronger ~O($M^{1.4}$) scaling with the number of monomers. Figure 5 reports the computational time associated with the various parts of the gradient evaluation as a function of the number of water monomers. For the $n < 6$ clusters, the most time-consuming part of the gradient evaluation involves the derivatives of the repulsive potential, but for larger clusters, the derivatives of the induced dipole moment term dominate the gradient evaluation. The latter derivatives can be expressed as

$$\frac{\partial V_{\text{ind}}}{\partial R_k} = \frac{\partial}{\partial R_k}\sum_j \frac{\boldsymbol{\mu}_j \cdot \mathbf{r}_j}{r_j^3} = \sum_j \boldsymbol{\mu}_j \cdot \frac{\partial}{\partial R_k}\left(\frac{\mathbf{r}_j}{r_j^3}\right) + \sum_j \frac{\mathbf{r}_j}{r_j^3} \cdot \frac{\partial \boldsymbol{\mu}_j}{\partial R_k} \tag{6}$$

where the subscript k denotes the atomic coordinates and $\boldsymbol{\mu}_j$ is the induced dipole moment located at the M site of the jth molecule. The first term on the right-hand side of equation. Equation 6 can be expanded as

$$\begin{aligned}\sum_j \boldsymbol{\mu}_j \cdot \frac{\partial}{\partial R_k}\left(\frac{\mathbf{r}_j}{r_j^3}\right) &= \sum_j \mu_{xj}\frac{\partial}{\partial R_k}\left(\frac{r_{xj}}{r_j^3}\right) + \mu_{yj}\frac{\partial}{\partial R_k}\left(\frac{r_{yj}}{r_j^3}\right) + \mu_{zj}\frac{\partial}{\partial R_k}\left(\frac{r_{zj}}{r_j^3}\right) \\ &= \mu_{xk}\frac{\partial}{\partial R_k}\left(\frac{r_{xk}}{r_k^3}\right) + \mu_{yk}\frac{\partial}{\partial R_k}\left(\frac{r_{yk}}{r_k^3}\right) + \mu_{zk}\frac{\partial}{\partial R_k}\left(\frac{r_{zk}}{r_k^3}\right)\end{aligned} \tag{7}$$

Only the term with $k = j$ is nonzero, making the evaluation of this contribution to the gradient computationally fast. However, the second term on the right-hand side of equation. Equation 6, which can be expanded as

$$\sum_j \frac{\mathbf{r}_j}{r_j^3} \cdot \frac{\partial \boldsymbol{\mu}_j}{\partial R_k} = \sum_j \left[\left(\frac{r_{xj}}{r_j^3}\right)\frac{\partial \mu_{xj}}{\partial R_k} + \left(\frac{r_{yj}}{r_j^3}\right)\frac{\partial \mu_{yj}}{\partial R_k} + \left(\frac{r_{zj}}{r_j^3}\right)\frac{\partial \mu_{zj}}{\partial R_k}\right] \tag{8}$$

does not undergo such a simplification. In the gradient evaluation, only the induced dipole moment term involves a sum over molecules. Of the clusters considered here the computational effort associated with the terms in equations. Equations 7 and 8 are O($M^{1.0}$) and O($M^{1.8}$), respectively. Hence for sufficiently large clusters, the gradient evaluation in the DVR approach will display a computational scaling approach O($M^{1.8}$). (Again this assumes the number of grid points does not grow with system size, which in most applications can be assured by use of a prescreening step.) In general, in the absence of prescreening, the number of grid points would grow linearly water system size giving in overall scaling of O($M^{2.8}$), the same as with the GTO basis set.

The OEPM-DVR code has been parallelized using structured loop-level parallelism implemented via OpenMP.[57] The energy gradient and potential energy computations contain computationally intensive data-parallel loops, parallelization of which is straightforward. The iterative Lanczos algorithm used to calculate the energy, on the other hand, is implemented via a sequential solver

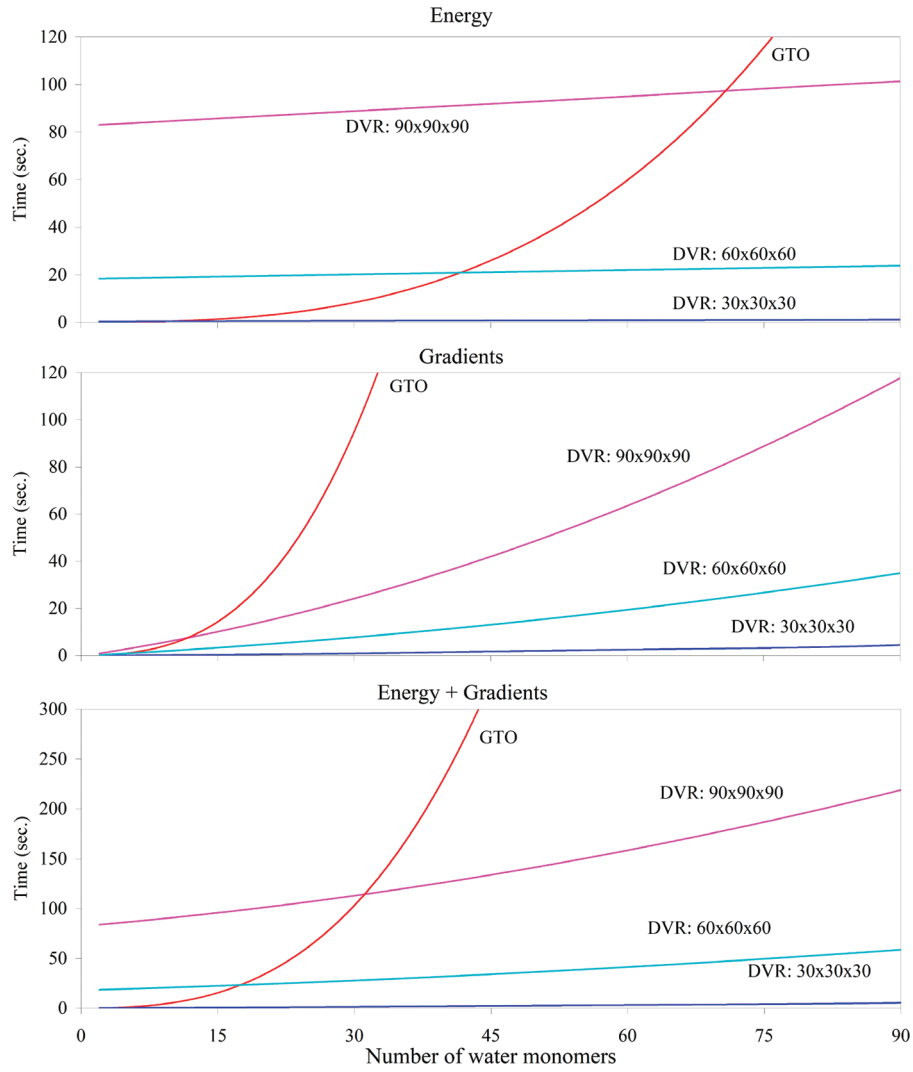

Figure 3. CPU time required to calculate the energy and gradient using GTO basis sets and three different DVR grids, 30 × 30 × 30, 60 × 60 × 60, and 90 × 90 × 90. The last graph shows the time of the energy and gradient together.

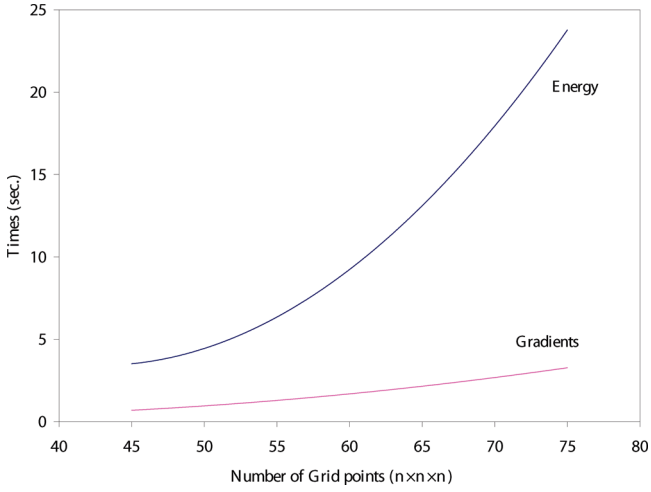

Figure 4. CPU time required to calculate the energy and gradients of a $(H_2O)_6^-$ cluster using 60 × 60 × 60 bohr box size. The number of grid points in the each direction is varied from 45 to 75.

library,[63] and the OpenMP parallelization was limited to only the eigenvector update stages during reverse communication with the solver.

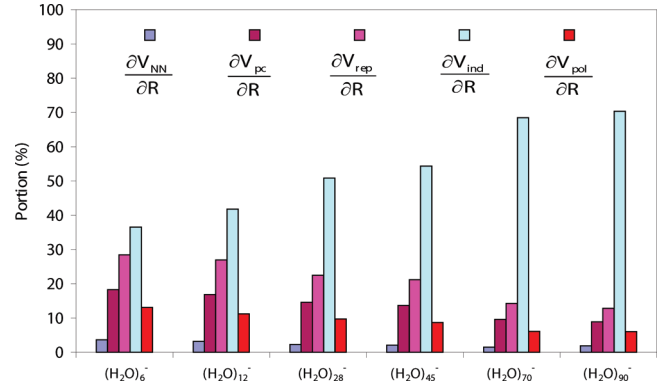

Figure 5. Relative CPU times for the various contributions to the gradient calculation.

Figure 6 reports the results of the parallel speed-up analysis. The runs are made on a SGI Altix 4700 shared-memory system. For the speedup analysis the energy and gradient for the $(H_2O)_{45}^-$ cluster are calculated using a 60 × 60 × 60 DVR grid. Figure 6 shows the normalized wall-time for various sections of the code as well as the overall run. Near-perfect speed-up is obtained for the potential energy and the gradient computations, while the diagonal-

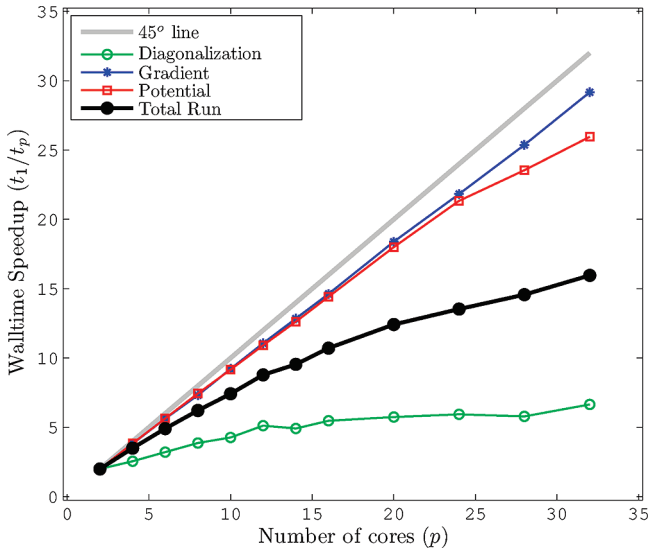

Figure 6. Parallel speed-up analysis of $(H_2O)_{45}^-$ cluster using a 60 × 60 × 60 DVR grid.

ization step does not perform well beyond 12 cores. For $(H_2O)_{45}^-$, the computer time to evaluate the enery exceeds that for the gradient, causing the efficiency of the parallelization of the energy plus gradient to perform poorly on over 12 CPUs as well. However, the computational effort to evaluate the gradient grows more rapidly with increasing cluster size than the time to evaluate the energy (see Figure 3), and for $(H_2O)_{90}^-$ the scaling of the parallelization is quite good up to about 32 cores. As a result nanosecond MD simulations are now possible on large $(H_2O)_n^-$ clusters using the OEPM approach even with the inclusions of interaction with the induced dipoles.

5. Conclusions

In this work, a sine-type DVR basis implementation of the one-electron polarization model for $(H_2O)_n^-$ clusters developed in our group has been described. Even with a grid as large as 60 × 60 × 60 [equivalent to 216 000 sine basis functions], the gradient calculations with the DVR approach are computationally faster than those using the GTO basis sets for clusters, containing more than 12 monomers.

The sine-type particle-in-the-box basis set, generates a uniform set of grid points. Significant computational savings could be achieved by using nonuniform grids, in particular using a sparser density of points in regions of space, where the electron density is relatively low. Exploratory calculations with harmonic oscillator DVR grids, in which the distance between grid points grows with increasing distance from the center of the box, shows that with such grids it is possible to achieve about an order of magnitude reduction in the CPU time required to evaluate the energy and gradients in the DVR approach with no loss of accuracy.

Acknowledgment. The authors acknowledge helpful discussions with Jing Ding. This research was carried out with support from the National Science Foundation under grant number CHE-0809457. T.S. acknowledges the donors of The American Chemical Society Petroleum Research Fund for support of this research through grant PRF no. 47344-GB6. The calculations were carried out on computers in the University of Pittsburgh's Center for Molecular and Materials Simulations and the Pittsburgh Supercomputing Center.

References

(1) Kim, K. S.; Park, I.; Lee, S.; Cho, K.; Lee, J. Y.; Kim, J.; Joannopoulos, J. D. *Phys. Rev. Lett.* **1995**, *76*, 956.

(2) Paik, D. H.; Lee, I. R.; Yang, D. S.; Baskin, J. S.; Zewail, A. H. *Science* **2004**, *306*, 672.

(3) Hammer, N. I.; Shin, J. W.; Headrick, J. M.; Kiden, E. G.; Roscioli, J. R.; Weddle, G. H.; Johnson, M. A. *Science* **2004**, *306*, 675.

(4) Jordan, K. D. *Science* **2004**, *306*, 618.

(5) Borgis, D.; Rossky, P. J.; Turi, L. *J. Chem. Phys.* **2006**, *125*, 064501.

(6) Coe, J. V.; Lee, G. H.; Eaton, J. G.; Arnold, S. T.; Sarkas, H. W.; Bowen, K. H.; Ludewigt, C.; Haberland, H.; Worsnop, D. R. *J. Chem. Phys.* **1990**, *92*, 3980.

(7) Verlet, J. R. R.; Bragg, A. E.; Kammrath, A.; Cheshnovsky, O.; Neumark, D. M. *Science* **2005**, *307*, 93.

(8) Bragg, A. E.; Verlet, J. R. R.; Kammrath, A.; Cheshnovsky, O.; Neumark, D. M. *Science* **2004**, *306*, 669.

(9) Hammer, N. I.; Roscioli, J. R.; Johnson, M. A.; Myshakin, E. M.; Jordan, K. D. *J. Phys. Chem. A* **2005**, *109*, 11526.

(10) Hammer, N. I.; Roscioli, J. R.; Johnson, M. A. *J. Phys. Chem. A* **2005**, *109*, 7896.

(11) Diken, E. G.; Robertson, W. H.; Johnson, M. A. *J. Phys. Chem. A* **2004**, *108*, 64.

(12) Hammer, N. I.; Roscioli, J. R.; Bopp, J. C.; Headrick, J. M.; Johnson, M. A. *J. Chem. Phys.* **2005**, *123*, 244311.

(13) Roscioli, J. R.; Hammer, N. I.; Johnson, M. A.; Diri, K.; Jordan, K. D. *J. Chem. Phys.* **2008**, *128*, 104314.

(14) Roscioli, J. R.; Johnson, M. A. *J. Chem. Phys.* **2007**, *126*, 024307.

(15) Haberland, H.; Schindler, H. G.; Worsnop, D. R. *Ber. Bunsen-Ges.* **1984**, *88*, 270.

(16) Haberland, H.; Ludewigt, C.; Schindler, H. G.; Worsnop, D. R. *J. Chem. Phys.* **1984**, *81*, 3742.

(17) Lee, H. M.; Suh, S. B.; Tarakeshwar, P.; Kim, K. S. *J. Chem. Phys.* **2005**, *122*, 044309.

(18) Suh, S. B.; Lee, H. M.; Kim, J.; Lee, J. Y.; Kim, K. S. *J. Chem. Phys.* **2000**, *113*, 5273.

(19) Lee, H. M.; Suh, S. B.; Kim, K. S. *J. Chem. Phys.* **2003**, *119*, 7685.

(20) Lee, H. M.; Lee, S.; Kim, K. S. *J. Chem. Phys.* **2003**, *119*, 187.

(21) Khan, A. *J. Mol. Struct.: THEOCHEM* **2008**, *850*, 144.

(22) Gutowski, M.; Skurski, P. *Recent Res. Dev. Phys. Chem.* **1999**, *3*, 245.

(23) Herbert, M. J.; Head-Gordon, M. *J. Phys. Chem. A* **2005**, *109*, 5217.

(24) Herbert, M. J.; Head-Gordon, M. *Phys. Chem. Chem. Phys.* **2006**, *8*, 68.

(25) Barnett, R. N.; Landman, U.; Cleveland, C. L.; Jortner, J. *J. Chem. Phys.* **1988**, *88*, 4429.

(26) Frigato, T.; VandeVondele, J.; Schmidt, B.; Schutte, C.; Jungwirth, P. *J. Phys. Chem. A* **2008**, *112*, 6125.

(27) Wallqvist, A.; Thirumalai, D.; Berne, B. J. *J. Chem. Phys.* **1986**, *85*, 1583.

(28) Wallqvist, A.; Thirumalai, D.; Berne, B. J. *J. Chem. Phys.* **1987**, *86*, 6404.

(29) Schnitker, J.; Rossky, P. J. *J. Chem. Phys.* **1987**, *86*, 3462.

(30) Turi, L.; Borgis, D. *J. Chem. Phys.* **2002**, *117*, 6186.

(31) Turi, L.; Sheu, W. S.; Rossky, P. J. *Science* **2005**, *309*, 914.

(32) Turi, L.; Madarasz, A.; Rossky, P. J. *J. Chem. Phys.* **2006**, *125*, 014308.

(33) Wang, F.; Jordan, K. D. *J. Chem. Phys.* **2002**, *116*, 6973.

(34) Wang, F.; Jordan, K. D. *J. Chem. Phys.* **2003**, *119*, 11645.

(35) Sommerfeld, T.; Jordan, K. D. *J. Phys. Chem. A* **2005**, *109*, 11531.

(36) Sommerfeld, T.; Jordan, K. D. *J. Am. Chem. Soc.* **2006**, *128*, 5828.

(37) Sommerfeld, T.; Gardner, S. D.; DeFusco, A.; Jordan, K. D. *J. Chem. Phys.* **2006**, *125*, 174301.

(38) DeFusco, A.; Sommerfeld, T.; Jordan, K. D. *Chem. Phys. Lett.* **2008**, *455*, 135.

(39) Sommerfeld, T.; DeFusco, A.; Jordan, K. D. *J. Phys. Chem. A* **2008**, *112*, 11021.

(40) Jacobson, L. D.; Williams, C. F.; Herbert, J. M. *J. Chem. Phys.* **2009**, *130*, 124115.

(41) Choi, T. H.; Jordan, K. D. *Chem. Phys. Lett.* **2008**, *464*, 139.

(42) Beck, M.; Jackle, A.; Worth, G.; Meyer, H.-D. *Phys. Rep.* **2000**, *324*, 1.

(43) Lill, J. V.; Parker, G. A.; Light, J. C. *Chem. Phys. Lett.* **1982**, *89*, 483.

(44) Light, J. C.; Hamilton, I. P.; Lill, J. V. *J. Chem. Phys.* **1985**, *82*, 1400.

(45) Baye, D.; Heenen, P.-H. *J. Phys. A* **1986**, *19*, 2041.

(46) Vincke, M.; Malegat, L.; Baye, D. *J. Phys. B* **1993**, *26*, 811.

(47) Szalay, V. *J. Chem. Phys.* **1993**, *99*, 1978.

(48) Szalay, V.; Nemes, L. *Chem. Phys. Lett.* **1994**, *231*, 225.

(49) Baye, D.; Hesse, M.; Vincke, M. *Phys. Rev. E* **2002**, *65*, 026701.

(50) Littlejohn, R. G.; Cargo, M.; Jr., T. C.; Mithell, K. A.; Poirier, B. *J. Chem. Phys.* **2002**, *116*, 8691.

(51) Littlejohn, R. G.; Cargo, M. *J. Chem. Phys.* **2002**, *116*, 7350.

(52) Schneider, B. I.; Nygaard, N. *Phys. Rev. E* **2004**, *70*, 056706.

(53) Buisseret, F.; Semay, C. *Phys. Rev. E* **2005**, *71*, 026705.

(54) Xiao, Y.; Poirier, B. *J. Theoret. Comput. Chem.* **2007**, *6*, 309.

(55) Rayson, M. J. *Phys. Rev. E* **2007**, *76*, 026704.

(56) Yan, D.; Peng, L.-Y.; Gong, Q. *Phys. Rev. E* **2009**, *79*, 036710.

(57) http://www.openmp.org. Accessed March, 2010.

(58) DeFusco, A.; Schofield, D.; Jordan, K. D. *Mol. Phys.* **2007**, *105*, 2681.

(59) Thole, B. T. *Chem. Phys.* **1981**, *59*, 341.

(60) Lanczos, C. J. *Res. Natl. Bur. Stand.* **1950**, *45*, 255.

(61) Pulay, P. *Mol. Phys.* **1969**, *17*, 197.

(62) Meyer, W.; Pulay, P. *J. Chem. Phys.* **1972**, *56*, 2109.

(63) Lehoucq, R. B.; Sorensen, D. C.; Yang, C. *ARPACK Users' Guide: Solution of Large-Scale Eigenvalue Problems with Implicitly Restarted Arnoldi Methods*; SIAM: Philadelphia, PA, 1998.

CT100263R